Eur. Phys. J. B **54**, 67–72 (2006)
DOI: 10.1140/epjb/e2006-00419-y

THE EUROPEAN PHYSICAL JOURNAL B

Raman study of orbital mediated multiphonons in $RMnO_3$ (R = Pr,Sm,Eu,Tb,Y)

J. Laverdière[1,a], S. Jandl[1], A.A. Mukhin[2], and V.Yu. Ivanov[2]

[1] Département de Physique, Université de Sherbrooke, J1K 2R1 Sherbrooke, Canada
[2] General Physics Institute, Russian Academy of Sciences, 119991 Moscow, Russia

Received 16 July 2006 / Received in final form 25 September 2006
Published online 29 November 2006 –

Abstract. We have studied $RMnO_3$ manganites (R = Pr, Sm, Eu, Tb, Y) Raman excitations in the 200–2800 cm^{-1} range as a function of temperature. Combinations of phonon energies are observed up to the fourth order, indicating the presence of electron-phonon coupling. In comparison to Γ-point phonon combinations, double phonon excitations appear to be blue shifted in large size rare earth ion compounds. The phonon combination intensities decrease rapidly with their increasing order, confirming other studies which conclude that the electron-phonon coupling is not as strong as supposed in the localized limit. Moreover, different intensity order dependences are observed between the phonon combination and the so-called Jahn-Teller mode. These effects are better described in the orbiton-phonon coupling scheme.

PACS. 78.30.-j Infrared and Raman spectra – 71.38.-k Polarons and electron-phonon interactions – 75.47.Lx manganites

1 Introduction

Since experimental evidence for orbital ordering has been reported in perovskite manganites [1], a debate sparked on the nature of orbital excitations predicted to appear in light scattering process [2]. Being only a theoretical discussion before 2001, Saitoh et al. [3] claimed that orbital excitations are observed in $LaMnO_3$ Raman spectra, showing three broad structures around 1000, 1160 and 1280 cm^{-1}. The theory supporting their measurements, based on electron-electron (e–e) interactions, excludes electron-phonon (e–p) coupling [4] and, since then, has been challenged by other models.

In contrast to exclusive e–e exchange interactions, Allen and Perebeinos [5] took into account a strong e–p coupling and an infinite Coulomb repulsion that prevents orbiton dispersion (localized limit). In this case, the orbiton corresponds to an exciton trapped by the local rearrangement of the Jahn-Teller (JT) distortion associated to a Franck-Condon effect that leads to strong multiphonon features. The multiphonon process was dismissed by Saitoh et al. [3] arguing that no phonon combinations could reproduce the high energy measured excitations, and that the orbiton temperature behavior differs from the phonon's. Afterwards, combinations have been proposed by different groups [6–8], using a low intensity mode around 650 cm^{-1}. Krüger et al. [7] showed that a resonance of this mode and its double occurs when laser energy is around the JT gap and Mn-Mn gap predicted respectively around 1.9 eV and 4.2 eV in $LaMnO_3$ [5]. Martín-Carrón and de Andrés [8] also measured phonon and multiphonon intensities ratios smaller than Allen and Perebeinos predictions [9]. Nevertheless, they concluded to a Franck-Condon multiphonon process showing that this ratio is constant with temperature, in agreement with the multiphonon theory [10].

A third approach, proposed by van den Brink [11], couples the orbiton to the lattice with an intermediate e–p coupling strength. As a result, phonon and orbiton characters are mixed and the phonon pattern repeats at regular interval of $w_0 \sim 650$ cm^{-1} (Q3 mode), also called the on-site JT vibration. Q3 mode corresponds to z-axis elongation and to in-plane contraction of the oxygen octahedron [12]. Franck-Condon satellites (multiphonons) are expected in higher energy range with lower intensities than in the strong coupling regime. Weak orbiton character structures are also predicted at $J_0/2 \sim 3/2\omega_0$. Manganites third order phonon processes have been reported in reference [8] for $LaMnO_3$, $PrMnO_3$, $HoMnO_3$ and hexagonal $YMnO_3$ and more recently in references [13] for $La_{1-x}Sr_xMnO_3$ ($x = 0, 0.06, 0.09, 0.125$) and in reference [14] for $Nd_{1-x}Sr_xMnO_3$ ($x = 0, 0.1, 0.5$). It has been pointed out by Choi et al. [13] and Jandl et al. [14] that

[a] e-mail: Jonathan.Laverdiere@USherbrooke.ca

the second to first order phonon intensity ratios behave in a different way than ordinary Franck-Condon process. Unlike the other phonon combinations, the JT vibration has weaker intensity than its own double combination. Doping dependent softening of multiphonon excitations has also been observed in $La_{1-x}Sr_xMnO_3$ by Choi et al. [13] with low doping. It has been interpreted as due to weakening of the e–p coupling and the decreasing JT gap with creation of orbital polarons. Doping dependent softening occurs with rapid decreasing intensity till suppression of second order signal which remains absent even for orbitally ordered $Nd_{0.5}Sr_{0.5}MnO_3$ [14].

Detailed phonon combinations haven't been proposed yet for higher energy structures. In this article, we study Raman active excitations of $PrMnO_3$, $SmMnO_3$, $EuMnO_3$, $TbMnO_3$ and $YMnO_3$, from room temperature down to 5 K in the 200–2800 cm^{-1} range. Differences in RE ionic sizes change JT distortions and Mn-O-Mn bond angle and influence the higher energy excitations. By choosing these compounds our objetcives are (1) to verify if we can combine first order phonons that reproduce high energy bands; (2) to evaluate if the phonon-orbiton interaction is important in the multiphonon excitations; and (3) to investigate the influence of the rare earth (RE) ion size, giving additional informations on the eventual orbital excitation character.

2 Experiment

The 0.5 cm^{-1} resolution Raman spectra have been performed in backscattering configuration using a Labram-800 microscope spectrometer equipped with a nitrogen cooled CCD detector. The sample was mounted on the cold finger of a micro-Helium Janis cryostat with the b direction or z-axis (Pnma symmetry) parallel to the incident radiation. All spectra were recorded by cooling down the sample. 632.8 nm (1.96 eV) He-Ne exciting line was used with a 10X (50X) objectives focusing on a 15 (3) μm diameter spots and keeping irradiance lower than $\sim$0.014 mW/(μm)^2 to avoid heating. $PrMnO_3$ and $SmMnO_3$ single crystals have been grown by the floating zone method [15]. Orthorhombic $YMnO_3$ samples were prepared under pressure as described in reference [16] and $EuMnO_3$, $TbMnO_3$ growth procedure is found in reference [17]. These last three samples were made of polycrystals randomly oriented. Nevertheless, we were able to specify the scattering plane and the relative polarization direction between the incident and the scattered light using the microscope setup that allows single crystals to be selected. Bomem Grams software [18] was used to fit the second order excitation data and subtract pure A_g and B_{2g} modes.

3 Experimental results and discussion

Figure 1 shows Raman active phonon spectra of $PrMnO_3$, $SmMnO_3$, $EuMnO_3$, $TbMnO_3$ and $YMnO_3$ (Pnma space group) for the incident light perpendicular to the xz plane and for the xx (A_g modes) and xz (B_{2g} modes) incident and scattered polarization configurations. Γ-Point phonon frequencies are collected in Table 1. The excitation reported in $LaMnO_3$ at 640 cm^{-1} [7,8] was measured using Raman [19,20] and infrared spectroscopies [21].

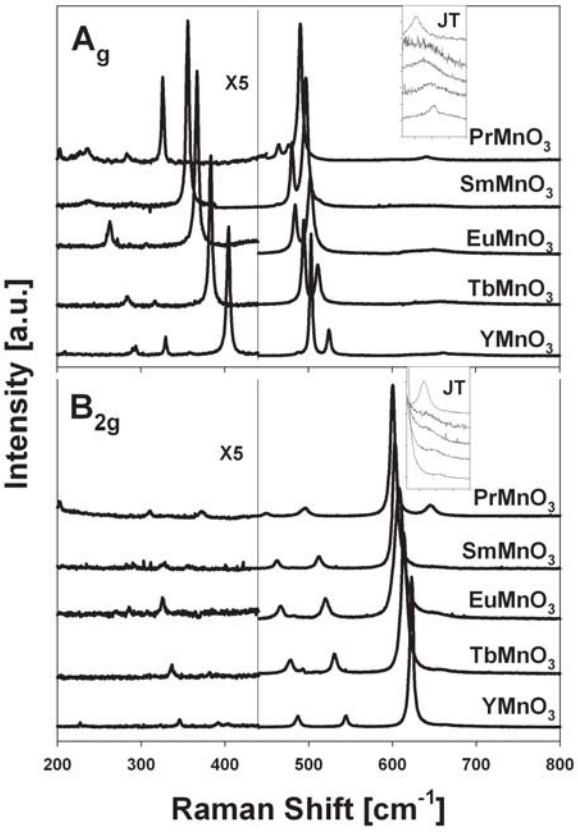

Fig. 1. Raman active phonon excitations at 5 K for $PrMnO_3$, $SmMnO_3$, $EuMnO_3$, $TbMnO_3$ and $YMnO_3$.

Table 1. Γ-Point Raman active phonon at 5K for $YMnO_3$, $SmMnO_3$, $PrMnO_3$, $EuMnO_3$ and $TbMnO_3$.

		$YMnO_3$	$TbMnO_3$	$EuMnO_3$	$SmMnO_3$	$PrMnO_3$
Γ-point Phonons		Frequencies (cm^{-1})	Frequencies (cm^{-1})	Frequencies (cm^{-1})	Frequencies (cm^{-1})	Frequencies (cm^{-1})
A_g	R(z)	192				
	$A_g(2)$	294	284	263	286	286
	$A_g(7)$	330	316	307	237	227
	$A_g(4)$	405	384	367	355	326
	$A_g(3)$	525	511	503	479	465
	$A_g(1)$	503	494	484	496	490
B_{2g}	R(x)	228		287		
	$B_{2g}(4)$	323	309	308	291	
	$B_{2g}(7)$	346	336	326	324	310
	$B_{2g}(3)$	488	478	466	460	450
	$B_{2g}(2)$	545	531	520	511	497
	$B_{2g}(1)$	623	614	608	606	600

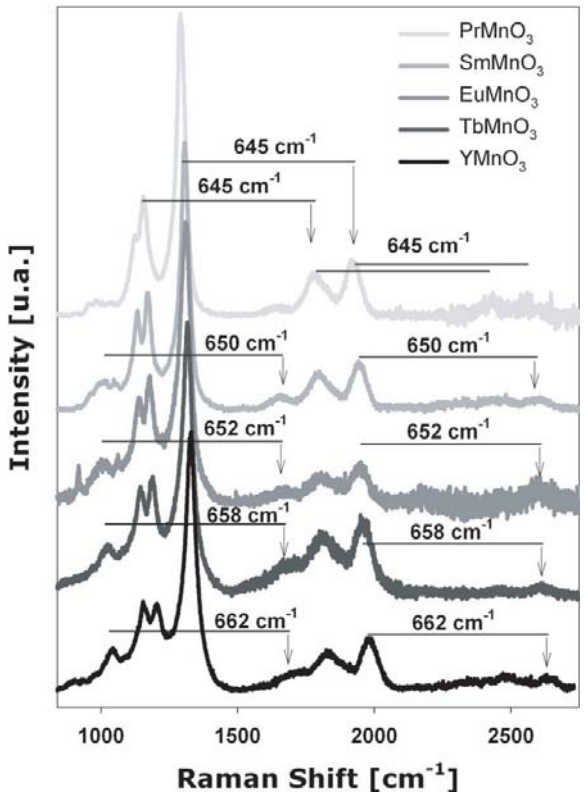

Fig. 2. Unpolarized spectra of Raman excitations in the 800–2800 cm^{-1} range at 5 K for $PrMnO_3$, $SmMnO_3$, $EuMnO_3$, $TbMnO_3$ and $YMnO_3$.

This excitation has been observed in $NdMnO_3$ at 645 cm^{-1} [14] and is also detected in $PrMnO_3$, $SmMnO_3$, $EuMnO_3$, $TbMnO_3$ and $YMnO_3$ around 646 cm^{-1}, 650 cm^{-1}, 652 cm^{-1}, 658 cm^{-1} and 662 cm^{-1} at 5 K respectively. The polarization spectra in Figure 1 indicate that such excitation is not a single mode but rather composed of an A_g and a B_g modes separated by 3 cm^{-1}. Rather than being assigned to a P*nma* normal phonon, it was associated with disorder density of states by some authors [16] or to on-site JT mode by others [11,13]. These last two pictures are not incompatible since on-site JT vibration could be a zone boundary phonon mode activated by orbital process instead of disorder.

Figure 2 shows Raman excitations in the 800–2500 cm^{-1} range at 5 K for $RMnO_3$ (R = Pr, Sm, Eu, Tb, Y). Structures below 1350 cm^{-1} excitation have been first associated with orbitons [3]. Figures 3a–3e show second order excitations for $PrMnO_3$, $SmMnO_3$, $EuMnO_3$, $TbMnO_3$ and $YMnO_3$ respectively. Fitted with mixed Gaussian and Lorentzian, the structures are identified by different numbers. An example for $YMnO_3$ fitting is shown in Figure 4. We can identify twelve different excitations in $PrMnO_3$ and $SmMnO_3$, thirteen in $EuMnO_3$ and $TbMnO_3$ and fifteen in $YMnO_3$. The numeration of the structures has been done by comparing the five compounds and by associating similar excitations with the same number. To elaborate Table 2, we have, in a first time, associated $YMnO_3$ second order excitations with possible combinations of Γ-Point numerous phonons (Fig. 1). We have afterwards calculated these same combinations for $PrMnO_3$, $SmMnO_3$, $EuMnO_3$ and $TbMnO_3$ and compared them to the measured excitations. We finally include in Table 2 the discrepancies ($\Delta\omega$) between Γ-Point combinations and the measured frequencies. Figure 5 shows the JT mode and phonon mode intensities logarithms as a function of the combination order for $PrMnO_3$, $SmMnO_3$ and $YMnO_3$. Phonon intensities represent the integrated intensities sum of the four phonons around 450 cm^{-1} for the first order and the group of structures around 1150, 1800 and 2450 cm^{-1} for the second, third and fourth orders respectively. First order JT mode is weaker than its double combination (at best 6 times weaker for $PrMnO_3$).

The four orbiton processes evoked (with their corresponding Holstein-Primakov boson polarizations) to explain the three peaks reported in $LaMnO_3$ [3] are simply not in sufficient number to explain the detected excitations in Figure 3. Moreover, as already reported [13,14], the high energy excitations are separated by the JT mode frequency (see Fig. 2), independently of the RE ions or their associated magnetic orders [22]. From possible combinations of the Γ-Point phonons (Table 2), one notes that lower energy multiphonon excitations (peaks #1 to #7) have increasing discrepancies with larger ionic radius (Y = 1.08 Å to Pr = 1.18 Å). This is in contrast with the JT double mode frequency that occurs with no significant disparities in all five compounds.

A strong e–p coupling as in the localized limit [5] would give a 1:2 intensity ratio between the one and two phonon processes. Similarly to $LaMnO_3$ [8,13], and $NdMnO_3$ [14], the relative intensities of the multiphonons with respect to the one-phonon peaks in our measurements do not verify such predictions measured at best ∼1:4 to 1:5 ratios in the case of 1300 cm^{-1} vs. 600 cm^{-1} mode intensity. Moreover, as a consequence of renormalization around the on-site JT mode frequency, here supposed to be the ∼650 cm^{-1} peak, we observe a predominance of this mode in the possible phonon combinations (Tab. 2). For the three compounds included in Figure 5, combinations of the JT mode intensities (triangles) increase remarkably between first and second order processes, as observed by Choi et al. [13] and Jandl et al. [14] in $LaMnO_3$ and $NdMnO_3$ respectively, then decrease faster at higher orders. Intensities associated with Franck-Condon processes should follow the power law g^n where g is the electron-phonon coupling constant and n the combination order [7]. Slopes in Figure 5 would lead to g values between 0.31 and 0.37 for the phonon structures and between 0.20 and 0.27 for the JT mode combinations reflecting a rather weak coupling.

The temperature dependences of 2×650 cm^{-1} and the ∼1300 cm^{-1} excitation are plotted in Figure 6 for $PrMnO_3$ and $YMnO_3$. Two remarks are noteworthy, first, even if the temperature behavior is not exactly the same, it follows the phonon's at low temperatures, especially in the $YMnO_3$ case. Second, the temperature anomaly observed by Saitoh et al. and confirmed by other groups [7,13] is also detected in $PrMnO_3$.

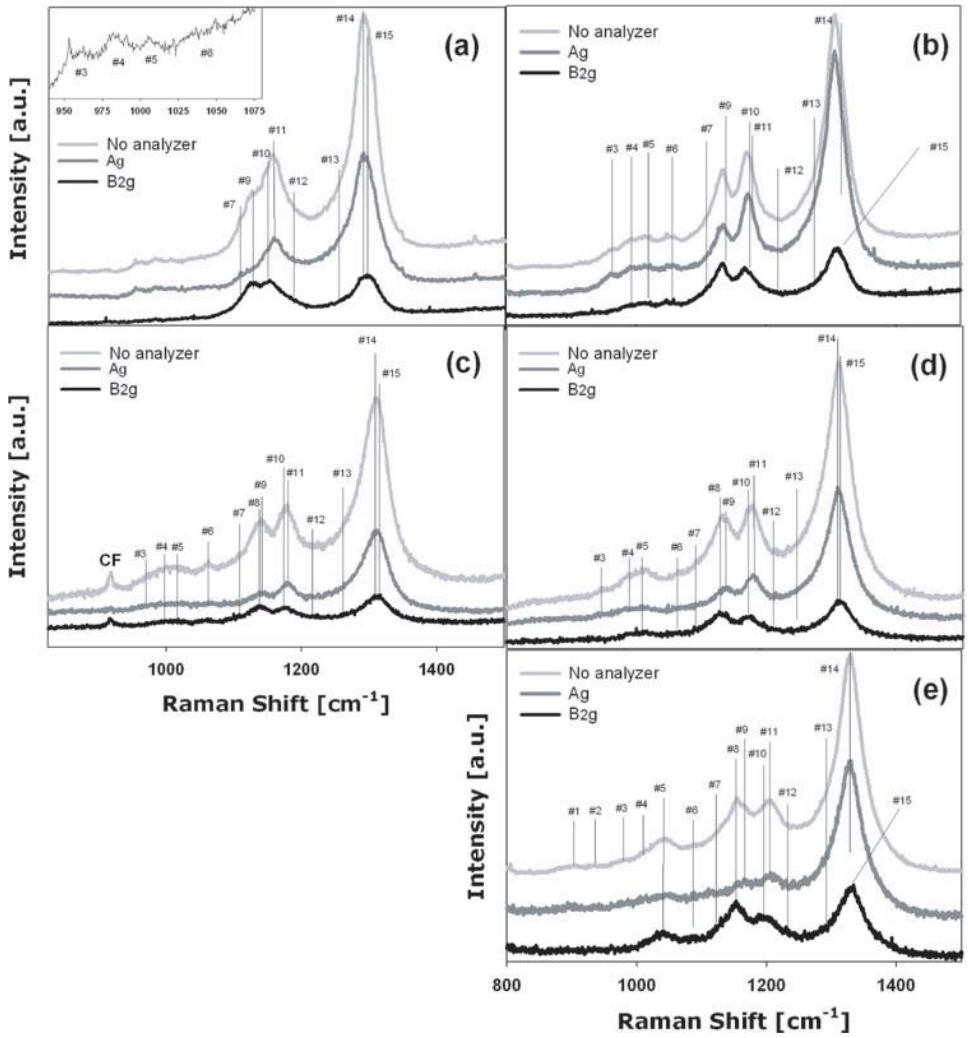

Fig. 3. Raman excitations in the 800 – 1500 cm^{-1} range at 5 K for (a) $PrMnO_3$, (b) $SmMnO_3$, (c) $EuMnO_3$, (d) $TbMnO_3$ and (e) $YMnO_3$.

Table 2. Γ-Point possible combinations at 5 K for $YMnO_3$, $SmMnO_3$, $PrMnO_3$, $EuMnO_3$ and $TbMnO_3$. * Indicates that $A_g(1)$ and $A_g(3)$ are exchanged in the combinations to take account of phonon mixing [17]; () indicate the energy difference between Γ-Point phonon combinations and measured multiphonon excitations.

		$YMnO_3$		$TbMnO_3$		$EuMnO_3$		$SmMnO_3$		$PrMnO_3$	
Peak	Possible Comb.	Γ-point (Δω) cm^{-1}	Measured Freq. cm^{-1}	Γ-point (Δω) cm^{-1}	Measured Freq. cm^{-1}	Γ-point (Δω) cm^{-1}	Measured Freq. cm^{-1}	Γ-point (Δω) cm^{-1}	Measured Freq. cm^{-1}	Γ-point (Δω) cm^{-1}	Measured Freq. cm^{-1}
#1	$B_{2g}(7)+B_{2g}(2)$ R(x) + JT	891(8) 890(9)	899 ± 3	867	---	846 939	---	835	---	807	---
#2	$A_g(4)+A_g(3)$	930(8)	938 ± 3	895	---	870	---	851*	---	816*	---
#3	2 X $B_{2g}(3)$	976(0)	976 ± 3	956(12)	968 ± 5	932(28)	960 ± 3	920(40)	960 ± 2	900(60)	960 ± 2
#4	$B_{2g}(7)$+JT	1008(1)	1009 ± 8	994(22)	1016 ± 6	978(7)	985 ± 3	973(16)	989 ± 3	955(31)	986 ± 4
#5	$A_g(1)+B_{2g}(2)$ 2 X $A_g(3)$	1048(-1) 1050(-3)	1047 ± 5	1025(5) 1022(8)	1030 ± 5	1004(15) 1006(13)	1019 ± 5	990*(24) 992*(22)	1014 ± 3	962*(41) 980*(23)	1003 ± 3
#6	2 X $B_{2g}(2)$	1090(0)	1090 ± 3	1062(19)	1081 ± 5	1040(20)	1060 ± 4	1022(28)	1050 ± 4	994(46)	1040 ± 10
#7	$A_g(1)+B_{2g}(1)$	1126(1)	1127 ± 3	1108(7)	1115 ± 5	1092(21)	1113 ± 3	1085*(31)	1116 ± 3	1065*(50)	1115 ± 3
#8	$B_{2g}(3)$+JT	1150(3)	1153 ± 3	1136(6)	1142	1118(20)	1138 ± 2	1109	---	1095	---
#9	$A_g(1)$+JT $B_{2g}(2)+B_{2g}(1)$	1165(1) 1168(-2)	1166 ± 3	1152(-3) 1145(4)	1149	1136(2) 1128(10)	1138 ± 2	1128*(5) 1117(16)	1133 ± 2	1110*(13) 1097(26)	1123 ± 3
#10	$A_g(3)$+JT	1187(8)	1195 ± 3	1169(14)	1183	1155(16)	1171 ± 3	1145*(23)	1168 ± 2	1135*(17)	1152 ± 3
#11	$B_{2g}(2)$+JT	1207(1)	1208 ± 6	1189(0)	1189	1172(6)	1178 ± 3	1160(12)	1172 ± 2	1142(18)	1160 ± 3
#12	2 X $B_{2g}(1)$	1246(1)	1247 ± 6	1228(4)	1224	1216(-2)	1214 ± 8	1212(-12)	1200 ± 8	1200(15)	1215 ± 8
#13	$B_{2g}(1)$+JT	1285(4)	1281 ± 4	1272(-1)	1271	1260(15)	1275 ± 5	1255(14)	1269 ± 5	1245(6)	1251 ± 5
#14	2 X JT	1324(4)	1328 ± 2	1316(0)	1316	1304(5)	1309 ± 2	1298(9)	1307 ± 2	1290(2)	1292 ± 2
#15	unknown	unknown	1331 ± 2	unknown	1318	unknown	1311 ± 2	unknown	1311 ± 2	unknown	1295 ± 2

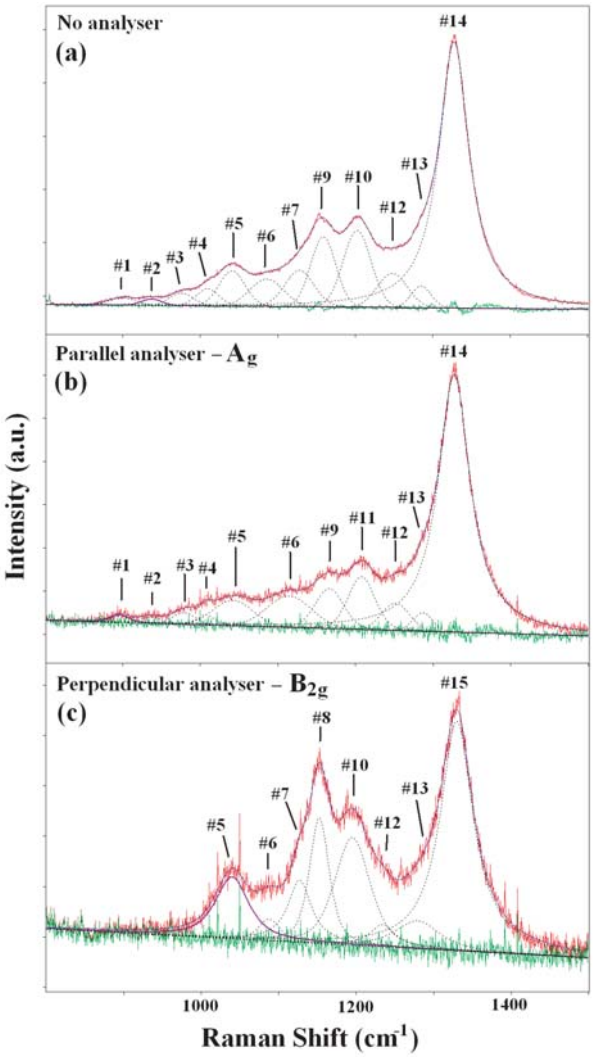

Fig. 4. Fitting of $YMnO_3$ second order Raman excitation. Spectra: with no analyzer (a), with analyzer parallel (b) and perpendicular (c) to the incident light polarization.

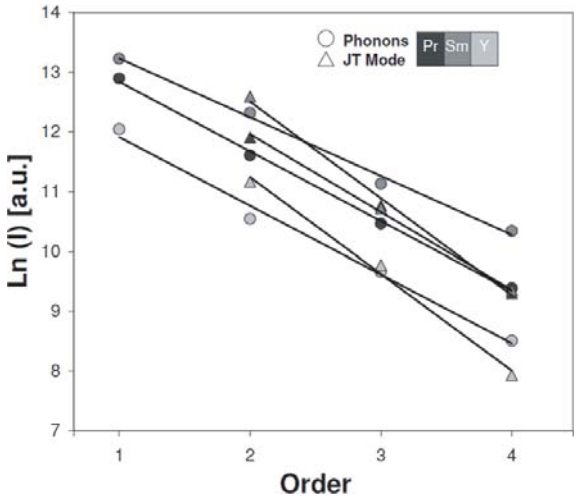

Fig. 5. Phonon and JT mode intensities logarithm for $PrMnO_3$, $SmMnO_3$ and $YMnO_3$ as a function of the combination order.

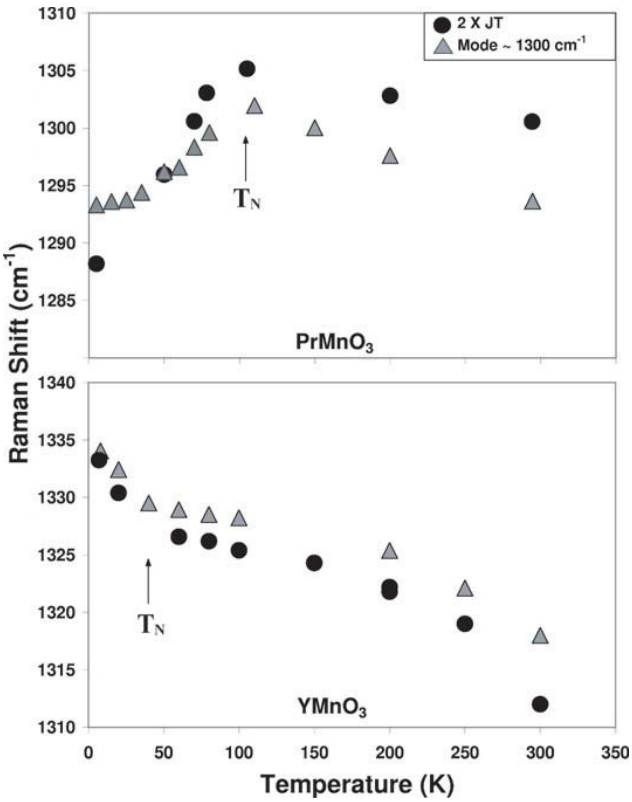

Fig. 6. Frequency temperature variation of the 1290 cm^{-1} excitation and the double of the ∼650 cm^{-1} on-site JT mode of $PrMnO_3$ and $YMnO_3$.

The 1290 cm^{-1} peak in A-type magnetic ordered $PrMnO_3$ has a stronger hardening than the 645 cm^{-1} double combination between room temperature and $T_N = 99$ K [23]. However, the opposite occurs below T_N, crossing the JT mode double combination around 50 K (see Fig. 6). Hardening is observed in the case of $YMnO_3$ in which IC-sinusoidal magnetic order is reported at $T_N = 42$ K [24]. Given that Γ-Point phonons are not exclusively involved in multiphonon scattering, $k \neq 0$ phonon combinations could be invoked. However, such combinations should not be affected by temperature or magnetic phase transitions as obviously observed in $PrMnO_3$. A possible explanation for discrepancies in the ∼650 and ∼1300 cm^{-1} temperature evolutions above T_N could be related to differences in orbital/phonon characters, 1300 cm^{-1} excitation being particularly influenced by orbiton renormalization.

The overall behavior of the combinations points to subtleties that contrast with a description relying exclusively on the Franck-Condon mechanism. Presence of a new mode (∼650 cm^{-1}) not predicted by the group analysis as well as excitation around $3\omega_0/2 \approx 975$ could reflect orbital-phonon renormalization as predicted by van den Brink approach [11]. Actually, orbital order in undoped

$RMnO_3$ perovskite manganites is of C-type [1]. It corresponds to alternate $3x^2 - r^2/3z^2 - r^2$ orbitals between neighboring Mn ions, with π/a electronic cloud modulation. Intuitively, zone boundary Q3 mode could couple with the C-type orbital order and become Raman active.

4 Conclusion

In this study, the Raman spectra of $PrMnO_3$, $SmMnO_3$, $EuMnO_3$, $TbMnO_3$ and $YMnO_3$, including first, second, third and fourth phonon orders, were performed and analyzed. The multiphonon processes occur in these compounds and seem to be a general property of $RMnO_3$ perovskite manganites. The particular excitation around 650 cm^{-1}, also called the on-site JT mode, reflects possible orbital contribution to multiphonon processes. JT mode is involved in most of the phonon combinations and its double frequency combination ($\sim$1300 cm^{-1}) is the most intense in the studied compounds. Γ-Point phonon combinations have been proposed from $YMnO_3$ and compared to $SmMnO_3$, $PrMnO_3$, $EuMnO_3$ and $TbMnO_3$ equivalent combinations that appear blueshifted. Such shifts could originate from orbiton renormalization, being stronger in large RE compounds. Also, multiple order intensity dependences indicate discrepancies between on-site JT mode combinations and phonon modes. In summary, our study shows subtleties in the high energy phonon processes that are better described in the orbiton-phonon coupling model.

We are grateful to M. Iliev for providing the Eu, Tb and Y samples. Also, this work was supported in part by the National Science and Engineering Research Council of Canada, the Fonds Québécois de la Recherche sur la Nature and in Moscow by the RFBR project No 06-02-17514.

References

1. Y. Murakami, J.P. Hill, D. Gibbs, M. Blume, I. Koyama, M. Tanaka, H. Kawata, T. Arima, Y. Tokura, K. Hirota, Y. Endoh, Phys. Rev. Lett. **81**, 582 (1998)
2. S. Ishihara, J. Inoue, S. Maekawa, Phys. Rev. B **55**, 8280 (1997)
3. E. Saitoh, S. Okamoto, K.T. Takahashi, K. Tobe, K. Yamamoto, T. Kimura, S. Ishihara, S. Maekawa, Y. Tokura, Nature **410**, 180 (2001)
4. S. Okamoto, S. Ishihara, S. Maekawa, Phys. Rev. B **66**, 014435 (2002)
5. P.B. Allen, V. Perebeinos, Phys. Rev. Lett. **92**, 4828 (1998)
6. M. Grüninger, R. Rückamp, M. Windt, P. Reutler, C. Zobel, T. Lorenz, A. Freimuth, A. Revcolevschi, Nature **39**, 418 (2002)
7. R. Krüger, B. Schulz, S. Naler, R. Rauer, D. Budelmann, J. Bäckström, K.H. Kim, S.-W. Cheong, V. Perebeinos, M. Rüsbhausen, Phys. Rev. Lett. **92**, 097203 (2004)
8. L. Martín-Carrón, A. de Andrés, Phys. Rev. Lett. **92**, 175501 (2004)
9. V. Perebeinos, P.B. Allen, Phys. Rev. B **92**, 4828 (1998)
10. M. Cardona, G. Güntherodt, *Topics in Applied Physics*, Vol. 50, Light Scattering in Solids II (Springer-Verlag, 1982)
11. J. van den Brink, Phys. Rev. Lett. **87**, 217202 (2001)
12. J. Kanamori, J. Appl. Phys. **31**, 14S (1960)
13. K.Y. Choi, P. Lemmens, G. Güntherodt, Yu.G. Pashkevich, V.P. Gnezdilov, P. Reutler, L. Pinsard-Gaudart, B. Büchner, A. Revcolevschi, Phys. Rev. B **72**, 024301 (2005)
14. S. Jandl, J. Laverdière, A.A. Mukhin, V.Yu. Ivanov, A.M. Balbashov, Physica B **381**, 214 (2006)
15. A.M. Balbashov, S.G. Karabashev, Y.A.M. Mukovskii, S.A. Zverkov, J. Cryst. Growth **167**, 365 (1996)
16. M.N. Iliev, B. Lorenz, A.P. Litvinchuk, Y.-Q. Wang, Y.Y. Sun, C.W. Chu, J. Phys.: Condens. Matter **17**, 3333 (2005)
17. M.N. Iliev, M.V. Abrashev, J. Laverdière, S. Jandl, M.M. Gospodinov, Y.-Q. Wang, Y.Y. Sun, Phys. Rev. B **73**, 064302 (2006)
18. Bomem Grams software, Galactic Industries Corporation
19. M.N. Iliev, M.V. Abrashev, H.G. Lee, V.N. Popov, Y.Y. Sun, C. Thomsen, R.L. Meng, C.W. Chu, Phys. Rev. B **57**, 2872 (1998)
20. E. Granado, A. García, J.A. Sanjurjo, C. Rettori, I. Torriani, F. Prado, R.D. Sánchez, A. Caneiro, S.B. Oseroff, Phys. Rev. B **60**, 11879 (1999)
21. A. Paolone, P. Roy, A. Pimenov, A. Loidl, O.K. Mel'nikov, A.Ya. Shapiro, Phys. Rev. B **61**, 11255 (1999)
22. T. Kimura, S. Ishihara, H. Shintani, T. Arima, K.T. Takahashi, K. Ishizaka, Y. Tokura, Phys. Rev. B **68**, 060403 (2003)
23. J. Hemberger, M. Brando, R. Wehn, V. Yu. Ivanov, A.A. Mukhin, A.M. Balbashov, A. Loidl, Phys. Rev. B **69**, 064418 (2004)
24. A. Munoz, J.A. Alonso, M.T. Casais, M.J. Martínez-Lope, J.L. Martínez, M.T. Fernández-Díaz, J. Phys.: Cond. Matt. **14**, 3285 (2002)